

PAPER • OPEN ACCESS

Challenges in Rotor Aerodynamic Modeling for Non-Uniform Inflow Conditions

To cite this article: K Boorsma et al 2024 J. Phys.: Conf. Ser. 2767 022006

View the article online for updates and enhancements.

You may also like

- A survey on integral equations for bioelectric modeling
 Guillermo Nuñez Ponasso
- Integral equations and boundary-element solution for static potential in a general piece-wise homogeneous volume conductor Matti Stenroos
- Comparison of contact conditions obtained by direct simulation with statistical analysis for normally distributed isotropic surfaces
 M Uchidate



doi:10.1088/1742-6596/2767/2/022006

Challenges in Rotor Aerodynamic Modeling for Non-Uniform Inflow Conditions

K Boorsma¹, J G Schepers¹, G R Pirrung², H A Madsen², N N Sørensen², C Grinderslev², G Bangga³, M Imiela⁴, A Croce⁵, S Cacciola⁵, F Blondel⁶, E Branlard⁷ and J Jonkman⁷

- ¹ Netherlands Organization for Applied Scientific Research (TNO), Petten, The Netherlands
- ² Technical University of Denmark (DTU), Roskilde, Denmark
- ³ Det Norske Veritas (DNV), Bristol, UK
- ⁴ German Aerospace Center (DLR), Braunschweig, Germany
- ⁵ Politecnico di Milano (POLIMI), Milano, Italy
- ⁶ French Institute of Petroleum (IFP) Energies nouvelles, Rueil-Malmaison, France
- National Renewable Energy Laboratory (NREL), Colorado, USA

E-mail: koen.boorsma@tno.nl

Abstract. Within an international collaboration framework, the accuracy of rotor aerodynamic models used for design load calculations of wind turbines is being assessed. Where the use of high-fidelity computation fluid dynamics (CFD) and mid-fidelity free-vortex wake (FVW) models has become commonplace within the wind energy community, these still fail to meet the requirements in terms of execution time and computational cost needed for design load calculations. The fast but engineering fidelity blade-element/momentum (BEM) method can therefore still be considered the industry workhorse for design load simulations.

At the same time, upscaling of wind turbine rotors makes inflow non-uniformities (e.g. shear, veer, turbulence) more important. The objective of this work is to assess model accuracy in non-uniform inflow conditions, which violate several BEM assumptions. Thereto a comparison in turbulent inflow has been executed including a wide variety of codes, focusing on the DanAero field measurements, where a 2.3-MW turbine was equipped with, among other sensors, a pressure measurement apparatus. The results indicate that, although average load patterns are in good agreement, this does not hold for the unsteady loads that drive fatigue damage and aero-elastic stability. A simplified comparison round in vertical shear was initiated to investigate the observed differences in a more controlled manner. A consistent offset in load amplitude was observed between CFD and free-vortex codes on the one hand and BEM-type codes on the other hand. To shed more light on the observations, dedicated efforts are ongoing to pinpoint the cause for these differences, in the end leading to guidelines for an improved BEM implementation.

1. Introduction

Within the framework of International Energy Agency (IEA) Wind Task 47 [1], an international consortium assesses the accuracy of rotor aerodynamic models used for wind turbine design. Here, measurement data from field tests and wind tunnels are used to validate the model predictions. This has been an ongoing effort for decades [2, 3, 4, 5, 6, 7, 8]. Although the use of high-fidelity computation fluid dynamics (CFD) and mid-fidelity free-vortex wake (FVW) models has become commonplace within the wind energy community, they still fail to meet the requirements in terms of execution time and computational cost needed for design load calculations. Therefore, the fast but engineering fidelity blade-element/momentum (BEM) method can therefore still be considered the industry workhorse for design load simulations. For uniform, constant inflow conditions and straight blades, the above-mentioned validation exercise has resulted in successful code validation, provided that the input is carefully selected, mitigating the 'human factor' [9]. Here, it is stressed that for a good agreement between CFD

Content from this work may be used under the terms of the Creative Commons Attribution 4.0 licence. Any further distribution of this work must maintain attribution to the author(s) and the title of the work, journal citation and DOI.

doi:10.1088/1742-6596/2767/2/022006

and lifting line models, it is required that the airfoil data fed to the lifting line codes is consistent with sectional predictions from CFD.

For non-uniform inflow conditions such as turbulent inflow, which is prescribed for fatigue load simulations, it has been less straightforward to achieve satisfactory agreement between simulations themselves [10, 11], as well as between predictions and measurements. At the same time, upscaling of wind turbine rotors has made these inflow non-uniformities (e.g. shear, veer, turbulence) more important. It is noted that the often unknown spatial and temporal distribution of the wind field complicates a consistent comparison against field measurements. In addition, inflow agreement between lifting line and CFD simulations is complicated by the different position of specifying the wind input, namely in the rotor plane or further upstream in the domain, respectively. Although engineering methodologies have been devised to circumvent this challenge [12], it remains impossible to achieve identical inflow conditions due to the propagation and convection of the wind field within the CFD domain and its interaction with the rotor.

From the modeling point of view, the one-dimensional axial momentum equation as implemented in BEM assumes that the inflow conditions are axi-symmetric (or uniform) with respect to the streamtube considered. In turbulent inflow conditions (or any other non-uniform inflow condition such as sheared or waked inflow), it may be clear that this is not the case. In addition, the influence of neighbouring elements and other blades are not taken into account in BEM theory and each annulus is treated independently. For a constant circulation distribution with span, this assumption could be justified, but in non-uniform inflow conditions, this is certainly not the case. Beside these shortcomings, engineering models for dynamic wake effects are found to dampen out rotor induction fluctuations due to inflow variations, depending on their implementation [13]. On the other hand, lifting line FVW methods also have their limitations, as for most of the vortex filament methods, the interaction between vorticity in the inflow and the wake is neglected [14].

The objective of this work is to assess model accuracy in non-uniform inflow conditions and to identify where improvements need to be made.

2. Methodology

The DanAero turbine has been a subject of investigation, which is a 80-m rotor diameter 2.3-MW wind turbine instrumented with, among others, surface pressure measurement equipment at four sections along the blade at 13, 19, 30 and 37 m from the rotor center [15] [16]. A detailed aero-elastic model description has been released that enables aero-elastic modeling of the turbine. Integrating the measured surface pressures around the sectional airfoil contour resulted in the chord-normal and tangential pressure forces at these four stations. Meteorological measurements were performed using a mast located 313 m (3.9 diameters) in the southwesterly direction (237°) upwind from the turbine. The meteorological mast included cup and sonic anemometers at 7 heights up to 93 m. More details about instrumentation can be found in [17]. The participants are summarized in Table 1, contributing by using a variety of rotor aerodynamic models ranging in fidelity from BEM to blade-resolved CFD. A wind field was generated using a constrained turbulence generator [34], which was fed with time-resolved meteorological mast measurements at seven different heights. A time series of approximately 400 s was selected with relatively constant rotational speed in partial load, i.e. without pitch angle variation, featuring an average axial induction factor of around 0.4 and angle of attack of 4 degrees at an 80% span. It is noted that the averaged operational and inflow conditions are identical to a previous comparison exercise in constant uniform inflow [9], which provides a foundation from which the current comparison exercise can be performed. Three different versions of this case are pursued as summarized in Table 2. A large number of partners then simulated the first test case with constant rotational speed and a flexible turbine model. For the lifting line codes, engineering

doi:10.1088/1742-6596/2767/2/022006

Table 1: High-level summary of participant codes and settings.

DNV_Bladed_BEM DNV Bladed BEM multi-body [18]	Legend Entry	Struc. Model I	nt Code Name	Ref.
DLR_TAUDLRTauRANSrigid[20]DTU_EllipSys3DDTUEllipSys3DRANSmulti-body[21,DTU_HAWC2DTUHAWC2BEMmulti-body[23,	DNV_Bladed_FVW DLR_TAU DTU_EllipSys3D DTU_HAWC2 DTU_HAWC2NW DTU_HAWC2NWVC IFPEN_BEM IFPEN_VL NREL_BEM NREL_OLAF PoliMi_Cp-Lambda TNOAero-BEM¹ TNOAero-BEM-S¹	multi-body rigid rigid multi-body [multi-body [wake multi-body [cylinder multi-body [TOR) multi-body [modal [multi-body []]	Bladed Tau EllipSys3D HAWC2 HAWC2 HAWC2 DeepLines Wind DeepLines Wind OpenFAST OpenFAST Cp-Lambda AeroModule AeroModule	[18, 19] [20] [21, 22] [23, 13] [24, 25] [26] [27] [27] [28] [29] [30] [31] [10]

¹ When coupled to the structural solver Phatas [33], the legend entry is PhatAero instead of TNOAero.

Table 2: Summary of mean conditions and configurations for the turbulent inflow rounds.

	Hub H. Wind Speed [m/s]		Rot. Speed [rpm]	Pitch [deg]	Ax. Ind. Factor [†] [-]	AOA^{\dagger} [deg]	
V1.1	6.1	7	13.2 (constant)	0.17	0.40	4	Flexible
V1.2	6.1	7	13.2 (constant)	3.00	0.25	2	Rigid
V1.3	6.1	7	13.2 (prescribed)	0.17	0.40	4	Flexible

 $^{^{\}dagger}$ estimate at 80% span using a BEM simulation

model extensions are used to account for dynamic wake effects, yawed flow, turbulent wake state, and dynamic stall and tower stagnation, and specific details can be inferred from the references given in Table 1. In addition to the lifting line codes, also CFD simulations were fed with the resulting wind field. However, the initial empty box CFD simulations suffered from unrealistic coherence (apparent from the synthetic turbulence generator), which resulted in a large variety between CFD codes for the propagated wind field at the rotor disk. Therefore, it was decided to exclude CFD simulations for this round.

Before comparing the simulation results, it was ensured that identical inflow was prescribed between the different codes by monitoring the wind speed at the hub and virtual probes corotating with the blades. After several iterations, good results were obtained by comparing both time series as well as statistics (average and standard deviation) of hub-height and blade probe wind speeds, confirming that the simulations are aligned, and slicing through the same wind field. This is illustrated in Figure 1 for the time series.

doi:10.1088/1742-6596/2767/2/022006

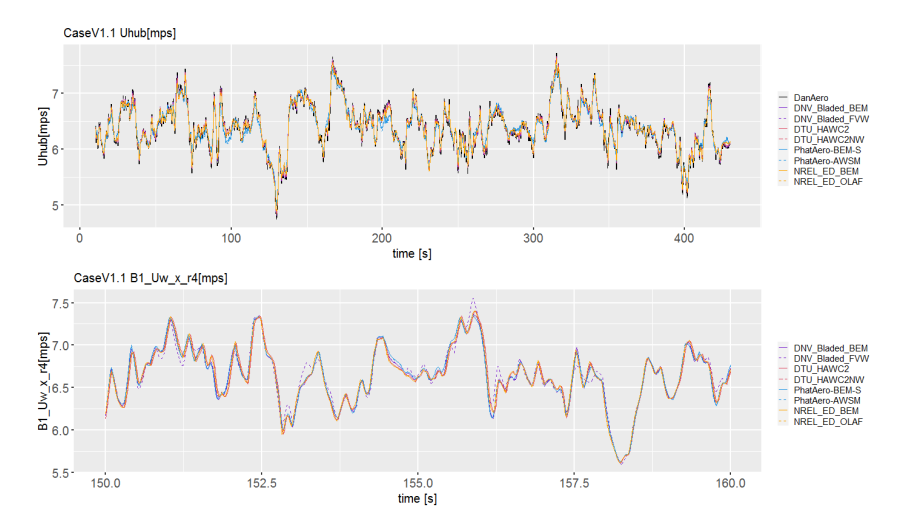


Figure 1: Illustration of alignment between the lifting line codes by means of hub-height wind speed (top) and undisturbed wind speed as registered by a virtual blade probe at 37 m from the rotor center (below).

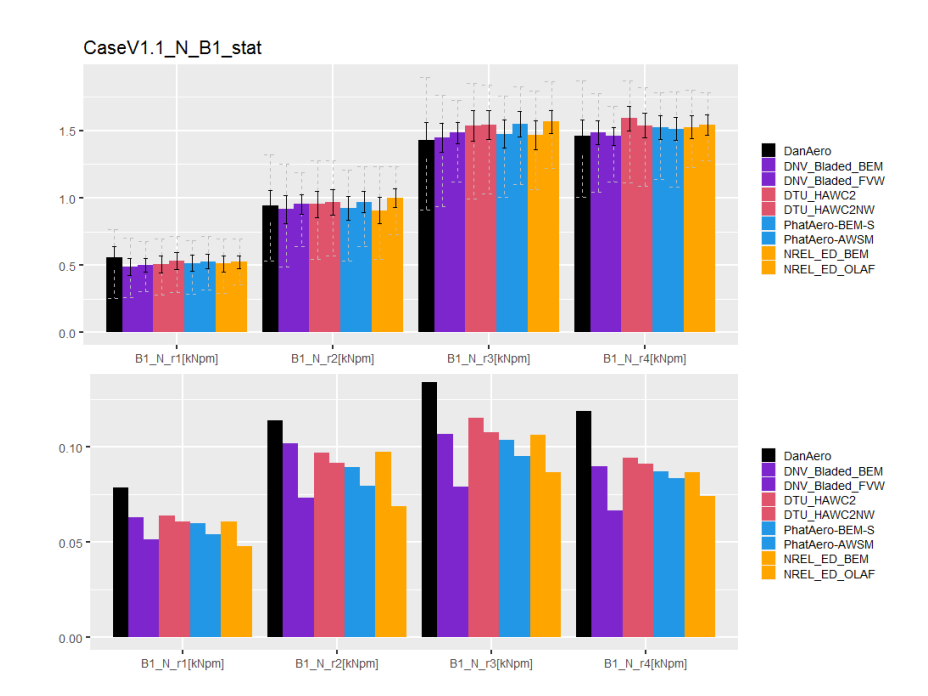


Figure 2: Comparison of measured and predicted normal force mean (top, standard deviation and extremes added by black and grey lines on top) and standard deviation (below) values at four radial stations 13 m, 19 m, 30 m and 37 m from the rotor center for case V1.1. The order of the bars in the plots agrees with the order of the legend entry.

3. Results in turbulent inflow

Figure 2 confirms a good agreement in average load levels, visualized by the normal force from the integrated pressure distributions at the four sections. However, the standard deviation shows a large spread between measurements and models but also between the models themselves. For the measurements, the standard deviation is obtained from the integrated pressure distributions. The disagreement with measurements regarding the normal force standard deviation can

doi:10.1088/1742-6596/2767/2/022006

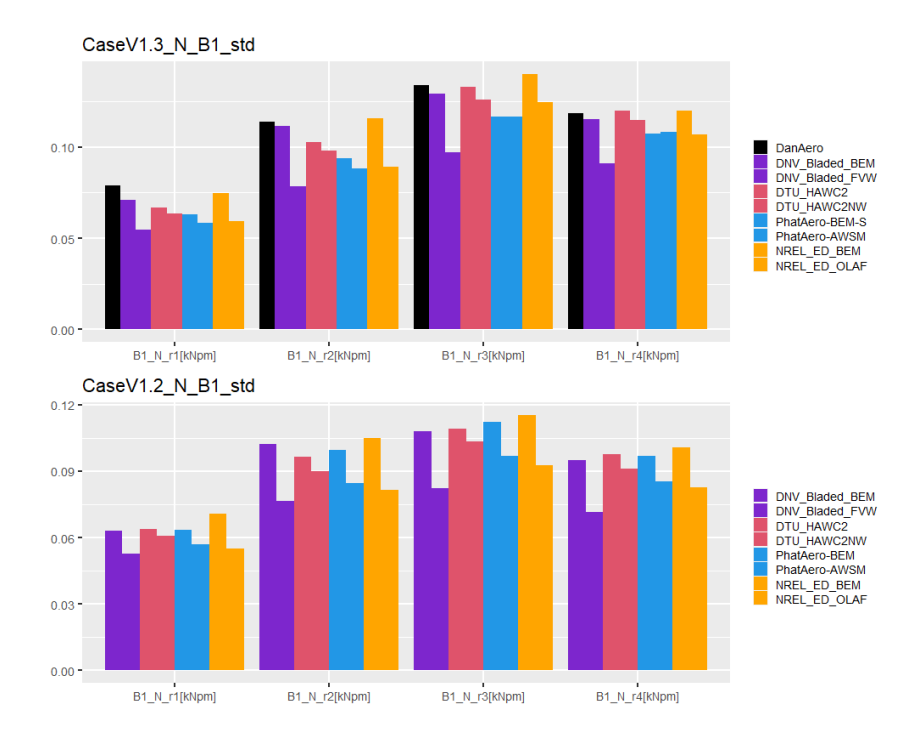


Figure 3: Comparison of measured and predicted normal force standard deviation for case V1.3 (top, prescribed rpm time series) and case V1.2 (bottom, lower induction, rigid case) at four radial stations 13 m, 19 m, 30 and 37 m from the rotor center. The order of the bars in the plots agrees with the order of the legend entry.

originate from a large number of causes. Engineering judgement points at poor representation of the inflow as only seven points were measured at the meteorological mast. To exclude the influence of rotor speed variations, an iteration was performed with prescribed rotor speed variations based on the measurements. Figure 3 illustrates that this case (V1.3) does bring the simulations closer to the measurements. A closer look at the underlying cause reveals that the predicted angle of attack and lift coefficient variations (judged by standard deviation) are hardly altered from case V1.1. to V1.3. This result indicates the increase in normal force variations is caused by the apparent dynamic pressure felt by the blades, which roughly scales with the square of rotor speed times local radius. What remains is the discrepancy between the normal force standard deviation predictions from the simulations, which feature large differences up to 20% for the FVW codes.

To further investigate the cause of these differences, a new computational case was defined comparing only model results between each other. It was decided to steer away from the turbulent wake state by increasing the blade pitch angle to 3 degrees, resulting in a lower axial induction factor. In addition to that, differences in structural modeling were excluded by prescribing a rigid turbine model, arriving at the definition of case V1.2. Despite these efforts, the resulting normal force standard deviations as depicted in the bottom part of Figure 3 still show large differences. A closer look reveals a consistent drop from BEM to FVW type codes, in line with previous investigations [10], which indicates the differences are originating from the aerodynamic modeling. This observation is further substantiated by the differences in unsteady axial induced velocities, as illustrated in Figure 4, featuring a difference in standard deviation up to a factor close to 3. The frequency content can be inspected by comparing the power spectral density of the axial induced velocity, which reveals the difference in standard deviation mainly to be caused by discrepancies at 1P (not shown here for the sake of brevity). However, also for

doi:10.1088/1742-6596/2767/2/022006

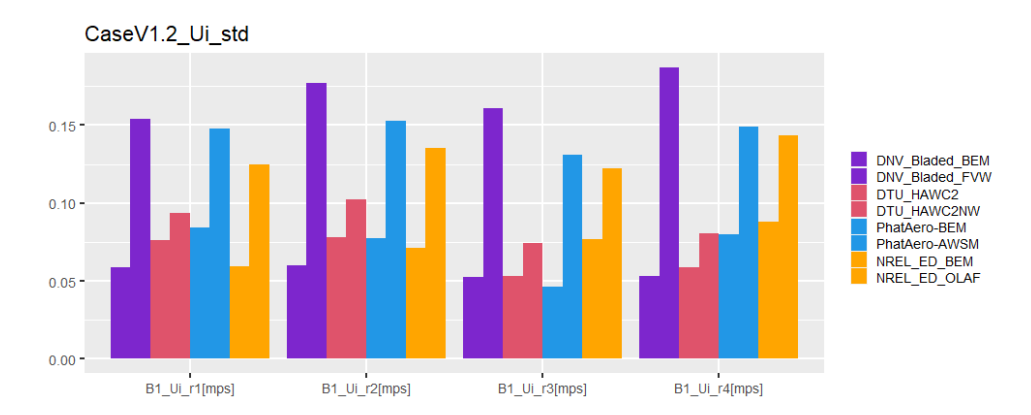


Figure 4: Comparison of the predicted standard deviation of axial-induced velocities for case V1.2 at four radial stations 13 m, 19 m, 30 m and 37 m from the rotor center. The order of the bars in the plot agrees with the order of the legend entry.

Table 3: Summary of mean conditions and configurations for the sheared inflow rounds.

	Hub H. Wind Speed [m/s]		-		Ax. Ind. Factor [†] [-]		
V1.4 V1.5		$0.35 \\ 0.35$	13.2 13.2	0.17 3.00	0.20	4 2	Rigid Rigid

[†] estimate at 80% span based on BEM simulations

the higher frequencies, more energy content can be observed for the FVW models. A deeper dive concluded that shed vorticity effects due to circulation variation in time are an important contributor to the high-frequency fluctuations observed in the FVW codes. For many of the BEM results, shed vorticity effects are also accounted for (e.g. by unsteady airfoil aerodynamic submodels [35]), but these are applied to force coefficients instead of induced velocities. To investigate the observed differences in a more controlled manner, a code comparison round in pure vertical shear was defined, allowing CFD contributions to be included more easily.

4. Sheared inflow investigation

4.1. Methodology

The hub-height wind speed was chosen to be identical to the mean value from the turbulent round, together with blade pitch angle and rotational speed, ensuring that angles of attack remain in attached flow without dynamic stall effects. However, care has to be taken to prevent differences due to the speed-up of the flow between the ground and the rotor (altering the effective shear profile), which is taken into account for the CFD simulations but not for the BEM simulations. Therefore, the hub height of the DanAero turbine was elevated to 100 m, which was verified by FVW simulations mirrored around ground level to be a safe distance not to alter the inflow field. A shear exponent of 0.35 was prescribed, resulting in a wind speed difference of 2 m/s between the top and bottom of the rotor plane. This is roughly equivalent to a shear exponent of 0.2 in combination with the original hub height of 57 m. In addition, the tower stagnation was not modeled to focus purely on the effect of shear. Table 3 summarizes the two cases, denoted as V1.4 and V1.5, which differ again in the loading of the rotor as illustrated by the axial induction factor.

doi:10.1088/1742-6596/2767/2/022006

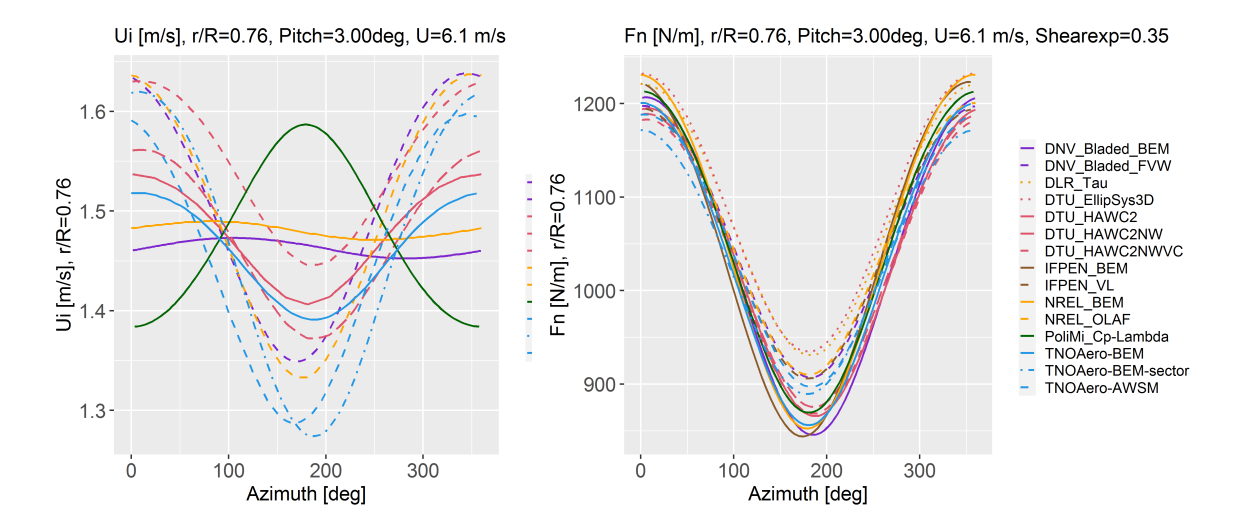


Figure 5: Comparison of the predicted variation of axial induced velocity (left) and chordnormal force (right) with rotor azimuth angle for case V1.5 at 37 m (76%R) from the rotor center. Solid lines represent BEM-type codes, dashed lines represent the FVW codes and dotted lines represent the CFD results.

4.2. Results

A selection of representative results in terms of azimuthal variation with shear is given in Figure 5. Although a visual inspection of the load variation with azimuth shows the expected dip for the blade pointing down, the variation of induced velocities (and hence also of angles of attack) reveal large scatter. Previous investigations in vertical shear have indicated a need for a local BEM implementation to match higher-fidelity model results [36], although the resulting load amplitudes were not compared quantitatively. The compared BEM implementations all feature a local evaluation of the momentum equations, but the specific implementations seem to differ significantly, resulting in different amplitudes and phases. The normal force and induced velocity amplitudes in Figure 6 are comparable to previous investigations [10], now featuring results from two CFD codes and five vortex wake models. Similar to the turbulent inflow comparison, load amplitudes are up to 20% higher for standard BEM-type codes in comparison to the FVW but also CFD models.

To shed more light on the observations, the lifting line code results have been re-processed to include local axial force coefficients (using normal and tangential forces) and local axial induction factors (using axial induced velocities). As such, the level of agreement with momentum theory can be assessed. The following two main options are pursued to perform this data reduction:

• Local

The local undisturbed wind speed at the quarter chord point is used to non-dimensionalize both the axial force and induced velocities at each radial station and azimuth angle.

• Annulus

The hub-height wind speed is used to non-dimensionalize both the axial force and induced velocities, which are first averaged over all azimuth angles to determine annulus averaged values. This technique then results in a separate value for each radial position only.

In addition, the axial induction factor should be corrected for the finite number of blades, hence it should not be the local value at the blade. For the BEM simulations, this is corrected by applying the Prandtl factor; however, this is less straightforward for the vortex wake codes. The same Prandtl factor distribution with radius has been applied to post-process all BEM and FVW

doi:10.1088/1742-6596/2767/2/022006

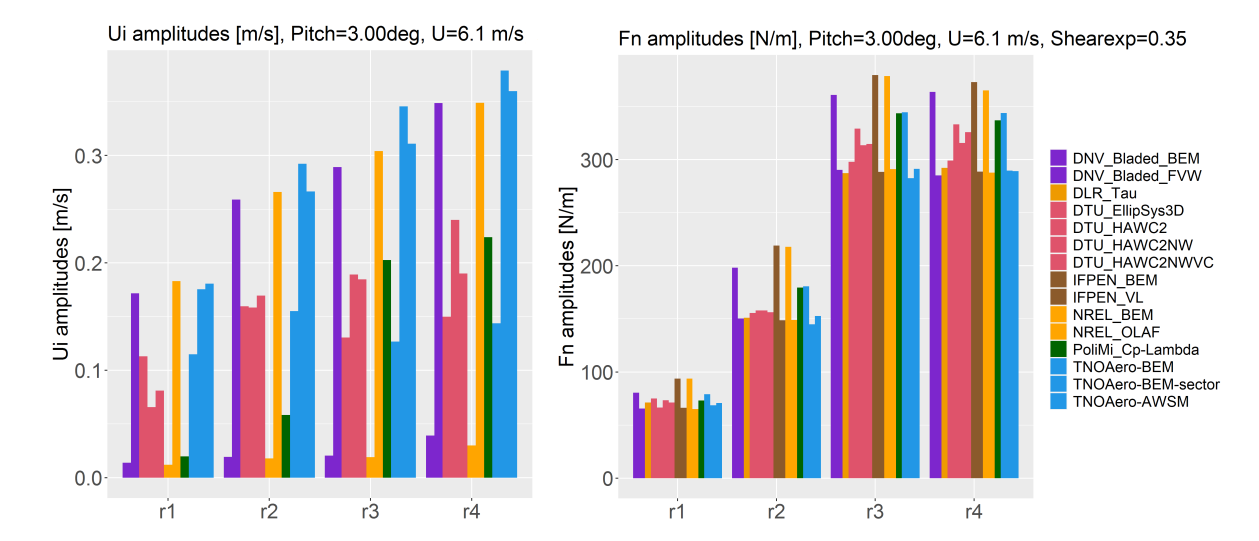


Figure 6: Comparison of amplitudes of axial induced velocity (left) and normal force (right) for sheared inflow (case V1.5). The order of the bars in the plots agrees with the order of the legend entry. Please note the two CFD codes (DLR_Tau and DTU_EllipSys3D) cannot provide lifting-line-induced velocities and are therefore omitted in the plot on the left-hand side.

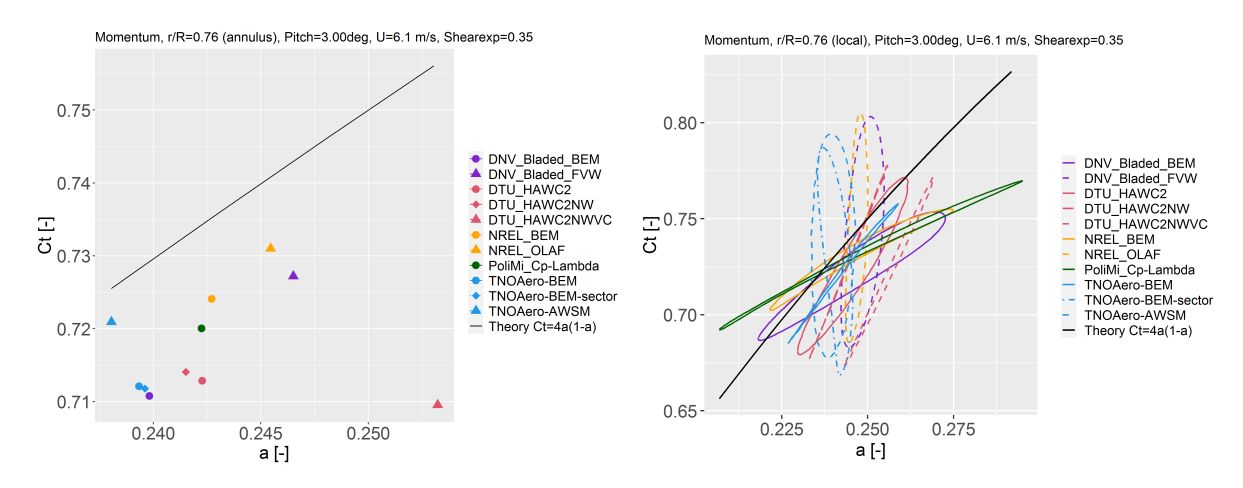


Figure 7: Comparison of agreement with the theoretical momentum curve for the annulus average (left) and local approach (right) (case V1.5 at 76%R).

code results, where it is noted that this largely affects the stations at 13 m and 37 m (33%R and 92%R). Also, for the inboard stations, the contribution of drag is significant for which the inclusion in momentum theory can be debated.

The resulting plots for case V1.5 at 76% R in Figure 7 show that it can be inferred that, despite some outliers, most codes seem close to annular momentum theory, as the scale of variation in the plot is rather small. For the local approach, this certainly is not the case. The FVW codes (dashed lines) seem to vary with rotor azimuth at a larger angle than the BEM results, compared to the direction of the local tangent of the momentum curve. Although there is a large variety between the BEM codes (solid lines), their variation seems to align with the direction of the momentum curve, which should be the case if a standard local BEM implementation has been applied. However, the loop of several BEM results, departing from the theoretical momentum curve, is still considerable. A closer look at the cause for these differences

doi:10.1088/1742-6596/2767/2/022006

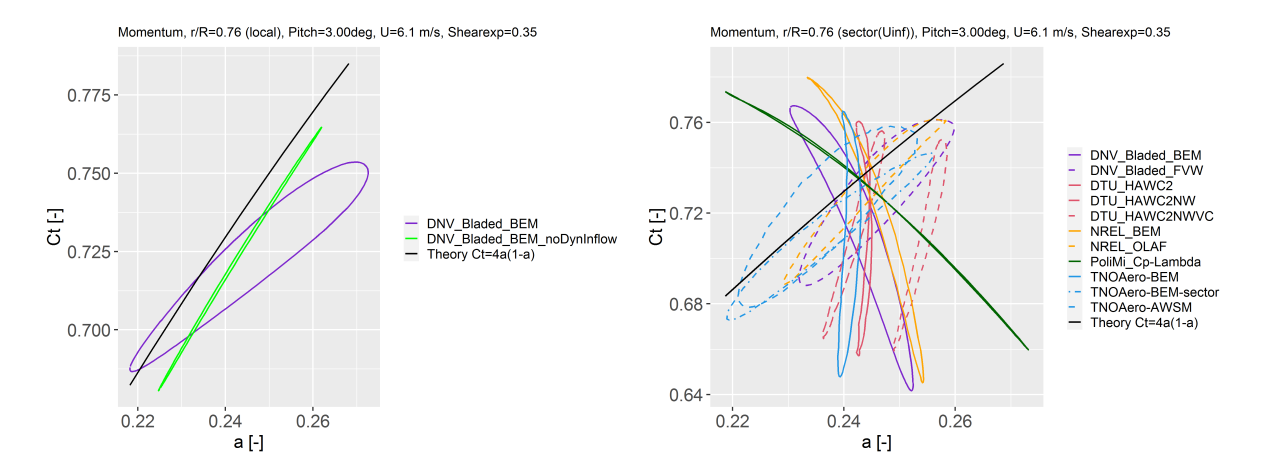


Figure 8: Comparison of agreement with the theoretical momentum curve for the local approach with and without the dynamic inflow model (left) and for sector averaging the reference wind speed over a 240-degree-wide annular sector (right) (case V1.5 at 76%R).

reveals engineering models that interfere with momentum equilibrium. It was found that some models predict a non-zero dynamic inflow inertia term for this sheared case, because of assumed proportionality to the time derivative of the local rather than the annulus averaged axial-induced velocity, the effect of which is illustrated in Figure 8. Also, decoupling the unsteady airfoil data correction from the induction calculation was found to potentially drive the results away from momentum equilibrium. Furthermore, it was verified that the difference in load amplitude between the vortex and BEM codes is not impacted by shed vorticity effects, which are typically modeled in the BEM codes and can be considered negligible for reduced frequencies around k=0.01.

The fact that the local momentum plots for FVW codes feature a loop that is systematically angled differently, compared to the slope of the theoretical momentum curve, questions the applicability of local momentum theory for non-uniform inflow conditions. Considering a full 360-degree annulus is balanced by the force of a finite number of blades, the representative free-stream velocity and axial force coefficient (as used in momentum theory), could be hypothesized to be averaged over an azimuthal sector. Post-processing the force and induction results in a sector-averaged reference wind speed, shown in Figure 8, which improves the agreement of vortex code results with the theoretical momentum curve. Implementation of this concept in a BEM code has been pursued in the TNOAero-BEM-sector results, which predicts results closer to FVW codes as illustrated in Figures 5 to 8. The observations and improvements are subject to further investigation and part of the ongoing efforts within IEA Wind Task 47.

5. Conclusions

An aero-elastic code comparison in turbulent inflow, focusing on the 2.3-MW DanAero field turbine, has been executed within the framework of IEA Wind Task 47, with contributions from a wide variety of aero-elastic codes. The results indicate that although average load patterns are in good agreement, this does not hold for the unsteady loads that drive fatigue damage and aero-elastic stability. A simplified comparison round in vertical shear was initiated to investigate the observed differences in a more controlled manner. A consistent offset in load amplitude was observed between CFD and FVW codes on the one hand and BEM-type codes on the other hand. To shed more light on the observations, dedicated efforts are ongoing to pinpoint the causes for these differences, leading to guidelines for an improved BEM implementation. The initial results point at improving the integration of engineering models and consideration of

doi:10.1088/1742-6596/2767/2/022006

momentum in sectors or azimuth averaging to pave the way forward.

Acknowledgments

The authors would like to thank IEA TCP Wind for facilitating Task 47 in their framework. The contributions of the participants to this task have been funded in various national programmes. The participants of the Danish DanAero project are acknowledged for providing the field measurement database. This work was authored in part by the National Renewable Energy Laboratory, operated by Alliance for Sustainable Energy, LLC, for the U.S. Department of Energy (DOE) under Contract No. DE-AC36-08GO28308. Funding provided by the U.S. Department of Energy Office of Energy Efficiency and Renewable Energy Wind Energy Technologies Office. The views expressed in the article do not necessarily represent the views of the DOE or the U.S. Government. The U.S. Government retains and the publisher, by accepting the article for publication, acknowledges that the U.S. Government retains a nonexclusive, paidup, irrevocable, worldwide license to publish or reproduce the published form of this work, or allow others to do so, for U.S. Government purposes. The Danish participation was funded by the Danish EUDP agency (J.nr. 64021-0015).

References

- [1] 2023 IEA TCP Wind website URL https://iea-wind.org/
- [2] Schepers J, Brand A, Bruining A, Graham J, Hand M, Infield D, Madsen H, Paynter J and Simms D 1997 Final Report of IEA Annex XIV: Field Rotor Aerodynamics Tech. Rep. ECN-C-97-027 Energy Research Centre of the Netherlands, ECN
- [3] Schepers J et al. 2002 Final report of IEA Annex XVIII' Enhanced Field Rotor Aerodynamics Database Tech. Rep. ECN-C-02-016 Energy Research Centre of the Netherlands, ECN
- [4] Schreck S 2008 IEA Wind Annex XX: HAWT Aerodynamics and Models from Wind Tunnel Measurements Tech. Rep. NREL/TP-500-43508 The National Renewable Energy Laboratory, NREL
- [5] Schepers J et al. 2012 Final report of IEA Task 29, Mexnext (Phase 1): Analysis of MEXICO wind tunnel measurements Tech. Rep. ECN-E-12-004 Energy Research Center of the Netherlands
- [6] Schepers J et al. 2014 Final report of IEA Task 29, Mexnext (Phase 2) Tech. Rep. ECN-E-14-060 Energy Research Center of the Netherlands
- [7] Boorsma K et al. 2018 Final report of IEA Task 29, Mexnext (Phase 3): Analysis of MEXICO wind tunnel measurements Tech. Rep. ECN-E-18-003 Energy Research Center of the Netherlands
- [8] Schepers J et al. 2021 IEA Wind TCP Task 29, (Phase IV): Detailed Aerodynamics of Wind Turbines Tech. rep. URL https://doi.org/10.5281/zenodo.4813068
- [9] Boorsma K et al. Progress in the validation of rotor aerodynamic codes using field data 2023 Wind Energy Science 8 211–230
- [10] Boorsma K, Wenz F, Lindenburg C, Aman M and Kloosterman M Validation and accommodation of vortex wake codes for wind turbine design load calculations 2020 Wind Energy Science 5 699-719
- [11] Perez-Becker S, Papi F, Saverin J, Marten D, Bianchini A and Paschereit C O Is the blade element momentum theory overestimating wind turbine loads? an aeroelastic comparison between openfast's aerodyn and qblade's lifting-line free vortex wake method 2020 Wind Energy Science 5 721–743
- [12] Wenz F, Boorsma K, Lutz T and Krämer E Cross-correlation-based approach to align turbulent inflow between cfd and lower-fidelity-codes in wind turbine simulations 2020 Journal of Physics: Conference Series 1618 062005
- [13] Madsen H A, Larsen T J, Pirrung G R, Ang L and Zahle F Implementation of the blade element momentum model on a polar grid and its aeroelastic load impact 2020 Wind Energy Science 5 1–27
- [14] Branlard E and Gaunaa M Impact of a wind turbine on turbulence: un-freezing the turbulence by means of a simple vortex particle approach 2016 Journal of Wind Engineering and Industrial Aerodynamics 151 37–47
- [15] Madsen H A, Bak C, Paulsen U S, Gaunaa M, Sørensen N N, Fuglsang P, Romblad J, Olsen N A, Enevoldsen P, Laursen J and Jensen L The dan-aero mw experiments 2010 48th Aiaa Aerospace Sciences Meeting Including the New Horizons Forum and Aerospace Exposition 2010–0645
- [16] Bak C et al. Dan-aero mw: Detailed aerodynamic measurements on a full scale mw wind turbine 2010 European Wind Energy Conference and Exhibition 2010, Ewec 2010 2 792–836
- [17] Bak C, Madsen H, Troldborg N, Gaunaa M, Skrzypinski W, Fischer A, Paulsen U, Møller R, Hansen

- P, Rasmussen M, and Fuglsang P 2013 DANAERO MW: Instrumentation of the NM80 turbine and meteorology mast at Tjæreborg Report-I-0083 DTU Wind Energy
- [18] Bangga G, Carrion M, Collier W and Parkinson S Technical modeling challenges for large idling wind turbines 2023 Journal of Physics: Conference Series 2626 012026
- [19] Bangga G, Parkinson S and Lutz T Utilizing high fidelity data into engineering model calculations for accurate wind turbine performance and load assessments under design load cases 2023 IET Renewable Power Generation 17 2909–2933
- [20] Schwamborn D, Gerhold T and Heinrich R 2006 The dlr tau-code: Recent applications in research and industry. European Conference on Computational Fluid Dynamics
- [21] Michelsen J 1992 Basis3d a platform for development of multiblock pde solvers. Tech. rep. Risø National Laboratory
- [22] Sørensen N 1995 General purpose flow solver applied to flow over hills. Ph.D. thesis
- [23] Madsen H, Bak C, Dossing M, Mikkelsen R and Oye S Validation and modification of the blade element momentum theory based on comparisons with actuator disc simulations 2010 Wind Energy 13 373–389 ISSN 10991824, 10954244
- [24] Pirrung G R, Aagaard Madsen H, Kim T and Heinz J C A coupled near and far wake model for wind turbine aerodynamics 2016 Wind Energy 19 2053–2069 ISSN 10991824, 10954244
- [25] Pirrung G, Riziotis V, Aagaard Madsen H, Hansen M and Kim T Comparison of a coupled near and far wake model with a free wake vortex code 2017 Wind Energy Science 2 15–33 ISSN 23667621, 23667451, 23667443
- [26] Li A, Gaunaa M, Pirrung G R and Horcas S G A computationally efficient engineering aerodynamic model for non-planar wind turbine rotors 2022 Wind Energy Science 7 75-104 URL https://wes.copernicus.org/articles/7/75/2022/
- [27] Le Cunff C et al. Fully Coupled Floating Wind Turbine Simulator Based on Nonlinear Finite Element Method:
 Part I Methodology 2013 nternational Conference on Ocean, Offshore and Arctic Engineering Volume
 8: Ocean Renewable Energy
- [28] Moriarty P J and Hansen A C 2005 Aerodyn theory manual Tech. rep. National Renewable Energy Laboratory NREL/EL-500-36881
- [29] Branlard E, Brownstein I, Strom B, Jonkman J et al. A multipurpose lifting-line flow solver for arbitrary wind energy concepts 2022 Wind Energy Science 7 455–467
- [30] Bauchau O, Bottasso C and Nikishkov Y Modeling rotorcraft dynamics with finite element multibody procedures 2001 Mathematical and Computer Modelling 33 1113 1137 ISSN 0895-7177 URL http://www.sciencedirect.com/science/article/pii/S0895717700003034
- [31] Boorsma K, Grasso F and Holierhoek J 2011 Enhanced approach for simulation of rotor aerodynamic loads Tech. Rep. ECN-M-12-003 ECN, presented at EWEA Offshore 2011, Amsterdam, 29 November 2011 - 1 December 2011
- [32] van Garrel A 2003 Development of a wind turbine aerodynamics simulation module Tech. Rep. ECN-C-03-079 ECN
- [33] Lindenburg C and Schepers J 2000 Phatas-IV aeroelastic modelling, release "dec-1999" and "nov-2000" Tech. Rep. ECN-CX-00-027 ECN
- [34] Rinker J M PyConTurb: An open-source constrained turbulence generator 2018 J. Phys.: Conf. Ser. 1037 062032 ISSN 1742-6596
- [35] Leishman JG and Beddoes TS 1998 "A Generalised model for unsteady airfoil behaviour and dynamic stall using the indicial method" 42th Annual Forum of the American Helicopter Society Washington DC
- [36] Madsen H A et al. Blade element momentum modeling of inflow with shear in comparison with advanced model results 2012 Wind Energy 15 63–81